ADVANCES IN ATMOSPHERIC SCIENCES, VOL. 29, NO. 2, 2012, 344–358

Radar Data Assimilation of the GRAPES Model and Experimental Results in a Typhoon Case

LIU Hongya*[1] (刘红亚), XUE Jishan[2] (薛纪善), GU Jianfeng[3] (顾建峰), and XU Haiming[4] (徐海明)

[1]*Shanghai Meteorological Center, Shanghai* 200030

[2]*State Key Laboratory of Severe Weather, Chinese Academy of Meteorological Sciences, Beijing* 100081

[3]*Chongqing Meteorological Bureau, Chongqing* 401147

[4]*Nanjing University of Information Science & Technology, Nanjing* 210044

(Received 12 May 2011; revised 19 September 2011)

ABSTRACT

Constructing β-mesoscale weather systems in initial fields remains a challenging problem in a mesoscale numerical weather prediction (NWP) model. Without vertical velocity matching the β-mesoscale weather system, convection activities would be suppressed by downdraft and cooling caused by precipitating hydrometeors. In this study, a method, basing on the three-dimensional variational (3DVAR) assimilation technique, was developed to obtain reasonable structures of β-mesoscale weather systems by assimilating radar data in a next-generation NWP system named GRAPES (the Global and Regional Assimilation and Prediction System) of China. Single-point testing indicated that assimilating radial wind significantly improved the horizontal wind but had little effect on the vertical velocity, while assimilating the retrieved vertical velocity (taking Richardson's equation as the observational operator) can greatly improve the vertical motion. Experiments on a typhoon show that assimilation of the radial wind data can greatly improve the prediction of the typhoon track, and can ameliorate precipitation to some extent. Assimilating the retrieved vertical velocity and rainwater mixing ratio, and adjusting water vapor and cloud water mixing ratio in the initial fields simultaneously, can significantly improve the tropical cyclone rainfall forecast but has little effect on typhoon path. Joint assimilating these three kinds of radar data gets the best results. Taking into account the scale of different weather systems and representation of observational data, data quality control, error setting of background field and observation data are still requiring further in-depth study.

Key words: 3DVAR mesoscale data assimilation, vertical velocity retrieval, Richardson's equation

Citation: Liu, H. Y., J. S. Xue, J. F. Gu, and H. M. Xu, 2012: Radar data assimilation of the GRAPES model and experimental results in a typhoon case. *Adv. Atmos. Sci.*, **29**(2), 344–358, doi: 10.1007/s00376-011-1063-y.

1. Introduction

The prediction of a mesoscale numerical weather prediction (NWP) model depends to a great extent on the initial conditions consisting of large and mesoscale information. Different from the NWP of synoptic scale systems, for which the initial conditions have been improved greatly due to the successful assimilation of the abundant satellite and other data, mesoscale NWPs still encounter difficulties modeling initial conditions that approach observations. Weather radars are unique in detecting features of cloud, precipitation, and wind fields of mesoscale weather systems with very high spatial and temporal resolutions. The assimilation of those data has been emphasized by a number of studies and operational development projects in recent years (Guo et al., 2000; Zupanski et al., 2002; Marecal and Mahfouf, 2003; Snyder and Zhang, 2003; Zhang et al., 2004; Sun, 2005a, b; Caya et al., 2005; Koizumi et al., 2005; Lee et al., 2010; Wang et al., 2010). In China, a network of more than 150 Doppler weather radars has been completed recently. The assimilation of the huge amount of data supplied by this costly network is an urgent task in the nation's meteorologic field

*Corresponding author: LIU Hongya, red_asia@163.com

(Xu et al., 2005; Gu et al., 2005; Wan et al., 2006). Although 3DVAR is not as excellent as four-dimensional variation (4DVAR) and Ensemble Kalman Filtering (EnKF) theoretically, 4DVAR and EnKF involve much higher computing costs and are not feasible for operational high-resolution models. The capability of radar data assimilation using the 3DVAR technique was demonstrated with the MM5 and WRF models by Xiao et al. (2005) and Xiao et al. (2007). Although their experiments showed positive impacts on rainfall forecasting, the analysis of vertical velocity in these studies was still on the order of centimeters per second and did not reflect β-mesoscale convective activities. Convection activities can be suppressed by downdraft and cooling caused by evaporation due to hydrometeor fallout if the magnitude of the vertical velocity does not match the scale of β-mesoscale weather system. The nudging technique (Hoke and Anthes, 1976; Liu et al., 2008b) was sought as a possible remedy to spin up the dynamical process prior to beginning the numerical prediction. Yang et al. (2009) combined the 3DVAR with a physical initialization (PI) method to assimilate radar data and significantly improved short-term rainfall prediction. Browning (1989) proposed several possible ways to advance the initial field of mesoscale NWP model, including (1) introducing more realistic distributions of vertical velocity and latent heating, improve moisture analysis, (2) adjusting the location and structure of mesoscale weather systems, and (3) advancing the impact of radiation balance by introducing the distribution of clouds. In this study, based on the characteristics of β-mesoscal weather systems and the advantages of radar data, a radar data assimilation scheme for GRAPES model was proposed and tested.

The organization of this paper is as follows. Section 2 gives a brief description of the GRAPES model. The radar data assimilation technique of the GRAPES model is described in detail in section 3. Section 4 provides the data assimilation results of a single radar observation test. Radar data assimilation and numerical simulation experiments on a real typhoon case are discussed in section 5. Finally, the main conclusions of this study are presented in section 6.

2. Description of GRAPES model and assimilation system

GRAPES is the next-generation, operational, nonhydrostatic NWP system of China. The prognostic variables of GRAPES include normalized pressure (Exner function) Π, potential temperature θ, three components of wind u, v, w, mixing ratio of water vapor $q_{\rm v}$, and other hydrometeors (i.e., cloud water $q_{\rm c}$, rain $q_{\rm r}$, cloud ice $q_{\rm i}$, snow $q_{\rm s}$, hail $q_{\rm h}$ and graupel $q_{\rm g}$). These variables were defined in the vertical coordinates of terrain following height with Charney-Phillips staggering. The variational data assimilation system retained the same definition of model prognostic variables, except that the hydrostatic assumption was applied. In the current operation assimilation system, the vertical velocity and hydrometeors were not analyzed, and the control variables were chosen as stream function, velocity potential, a choice between unbalanced normalized pressure or potential temperature, and a choice between specific or relative humidity. The linearized balance equation and geostrophic relation were used in the 3DVAR to relate wind increments to mass increments on η-surfaces. Empirical orthogonal functions (EOFs) were used for the vertical component of the background error covariance. Recursive filtering (RF) was applied to the horizontal increment fields of the control variables (Chen et al., 2008; Xue et al., 2008).

3. Radar data assimilation scheme

3.1 *Doppler radar radial velocity assimilation*

According to the principle of radar observation, the observation operator of Doppler radial velocity can be written as

$$V_{\rm r} = u\frac{x-x_i}{r_i} + v\frac{y-y_i}{r_i} + (w-v_{\rm T})\frac{z-z_i}{r_i} \qquad (1)$$

where $V_{\rm r}$ is the radial velocity, u, v, w are the three-dimensional wind fields of atmosphere; x, y, z are components of the radar site; x_i, y_i, z_i are components of the radar observation point; r_i is the distance from the radar to the observation point; $v_{\rm T}$ is the terminal velocity of raindrop.

3.2 *Inversion and assimilation of vertical velocity*

Radar reflectivity contains qualitative information about the vertical motion within a cloud. The vertical profile of vertical velocity in a cloud can be retrieved from radar reflectivity using statistical methods, but the statistical results usually vary with seasons, regions, and cloud types (Biggerstaff and Houze, 1991; Yuter and Houze, 1995; Kishore et al., 2005). This technique is often adopted by the physical initialization method in mesoscale models (Haase et al., 2000; Mcginley and Smart, 2001; Yuter and Houze, 2003; Milan et al., 2005). According to the statistical results of Yuter and Houze (1995), for a β-mesoscale weather system, the statistic profile of the vertical ve-

locity in a cloud can be written approximately in the following form

$$w = (\alpha \times (Z - Z_0) + \beta) \times e^{-(\gamma \times (H - H_0))^2} \quad (2)$$

where Z is the echo reflectivity, H is the elevation above the sea level, α=0.1, γ=0.4, β=0.3 m s^{-1}, Z_0=35 dBZ, H_0=6 km, and Z is the reflectivity $> Z_0$. By adjusting the parameters in the equation according to local weather features, users can get reasonable results. Figure 1 shows the vertical distribution of the vertical velocity at Z=55 dBZ; it is similar to the statistical results of Yuter and Houze (1995).

Richardson's equation (Richardson, 1922; Byrom and Roulstone, 2002) is used as an observation operator to assimilate the retrieved vertical velocity above

$$\gamma p \frac{\partial w}{\partial z} = \gamma p \left(\frac{Q}{T c_p} - \nabla \cdot V_\mathrm{h} \right) - V_\mathrm{h} \cdot \nabla p + g \int_z^\infty \nabla \cdot (\rho V_\mathrm{h}) dz \quad (3)$$

where c_p is the specific heat at constant pressure, c_v is the specific heat at constant volume, γ=c_p/c_v=1.4, p is the pressure, T is the temperature, z is the height, ρ is the air density, g is the acceleration due to gravity, Q is the diabatic heating rate per unit mass, V_h is the horizontal wind, and w is the vertical velocity.

Equation (3) determines the vertical gradient of w at height z and is derived by combining the continuity equation, the hydrostatic equation, and the thermodynamic equation. Ignoring the non-adiabatic item, Eq. (3) may be expressed with the state variables of GRAPES as

$$\gamma \Pi^\kappa \frac{\partial w}{\partial z} = -\left(u \frac{\partial \Pi^\kappa}{\partial x} + v \frac{\partial \Pi^\kappa}{\partial y} \right) - \gamma \Pi^\kappa \left(\frac{\partial u}{\partial x} + \frac{\partial v}{\partial y} \right) - \int_z^\infty \left[\frac{\partial}{\partial x} \left(\frac{\partial \Pi^\kappa}{\partial z} u \right) + \frac{\partial}{\partial y} \left(\frac{\partial \Pi^\kappa}{\partial z} v \right) \right] dz \,, \quad (4)$$

$$\Pi = \left(\frac{p}{P_0} \right)^{R/c_p} \,, \quad (5)$$

where R is the air constant, P_0=1000 hPa, κ=$c_p/R \approx$ 3.5, and Π is the Exner function.

Non-adiabatic heating comes mainly from radiation, surface sensible heating, and latent heating of water phase transformation. Latent heating plays a leading role for a β-mesoscale convective weather system. To calculate the latent heating, the condensation function is first used to obtain the condensation rate, and then the heating rate is derived. The equations

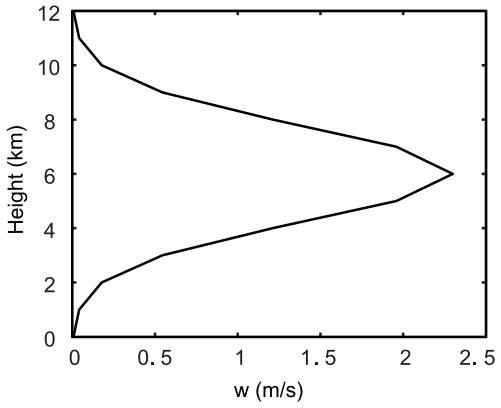

Fig. 1. Vertical profile of vertical velocity (w) calculated from the 55-dBZ reflectivity factor.

are as follows:

$$F = \frac{dq_\mathrm{vs}}{dp} = \frac{q_\mathrm{vs} T}{p} \left(\frac{L_\mathrm{v} R - c_p R_\mathrm{v} T}{c_p R_\mathrm{v} T^2 + (q_\mathrm{vs}/1000.0) L_\mathrm{v}^2} \right) , \quad (6)$$

$$C = -\frac{dq_\mathrm{vs}}{dt} = -F \frac{dp}{dt} = -F\omega = \rho g F w \,, \quad (7)$$

$$Q = L_\mathrm{v} C = \alpha w \,, \quad (8)$$

where F is the condensation function, C is the condensation rate, q_vs is the mixing ratio of saturated water vapor, L_v is the latent heat of evaporation, R_v is the constant of water vapor, ω is the vertical velocity in pressure coordinate, and α is a coefficient after a series of calculation.

3.3 *Adjust hydrometeors of initial field*

The mixing ratio of rainwater (q_r) was added as a control variable in the GRAPES-3DVAR system, and the relation between radar reflectivity and rainwater (Sun and Crook, 1997) is

$$Z = 43.1 + 17.5 \log(\rho q_\mathrm{r}) \,. \quad (9)$$

This relationship is relatively simple, and experimental results show that the assimilation of the derived rainwater from this relation is better than the assimilation of observed reflectivity (Sun and Crook, 1997; Sun and Crook, 1998). So, in the current study, we chose to assimilate rainwater.

Water vapor is essential in predicting precipitation, but weather radar cannot detect moisture. The usual practice is making the region where radar reflectivity reaches a certain threshold value saturated or constant. Assimilation results of this study show that the large reflectivities of radar echoes correspond to the ascending area at 500 hPa, and that the transition is very sharp between ascending and descending areas. Therefore, if the 500-hPa vertical velocity increment

was >0.3 m s^{-1}, the water vapor above lifting condensation level was set to saturation. A threshold of 0.3 m s^{-1} was used to exclude the ascending area caused by topographic forcing in non-echo areas.

Moreover, 10-cm wavelength radars are unable to detect small cloud particles. So, basing on warm rain scheme and under the assumption of stationary state, cloud water mixing ratio is diagnosed from vertical velocity and rainwater mixing ratio (Liu et al., 2008a).

4. Assimilation tests of single observation

In this part of the study, the three-dimensional structure of wind was examined by studying 3DVAR's response to a single observation from the radar (30.52°N, 114.38°E, 135.7 m) located at Wuhan, Hubei province of China. This observation was located at 30.28°N, 114.71°E, 4597.9 m elevation. The radar reflectivity was 40 dBZ, from which a vertical velocity of 1.095 m s^{-1} was obtained using Eq. (2). The radial velocity at the point was 17 m s^{-1}, away from the radar. The observation error of the radial wind and the retrieved vertical velocity were set to 5 m s^{-1} and 0.1 m s^{-1}, respectively. Because β-mesoscale systems usually have strong divergence and do not satisfy the geostrophic relations, the proportions of potential function and stream function, and of ageostrophic wind and geostrophic wind, were both adjusted to a ratio of 3:7 from the default setting of 1:9 (a value suitable for synoptic scale systems). Furthermore, the length scaling from background error of control variables were adjusted to 80 km from ∼500 km (a parameter for synoptic scale systems). The background field came from the 6-h forecast of operational numerical weather prediction system (T213) of National Meteorological Center (NMC) of China. The model horizontal mesh size was 0.1°×0.1°, and the model top was located at 35 km, with 32 non-equidistant vertical levels. Because convection occurs mainly in the troposphere, the vertical velocity calculation was only executed on the lower 1–15 layers (∼15 km). Interpolating the background variables to the observation point, we obtained u=10.3 m s^{-1}, v=1.65 m s^{-1}, $w = -7.4 \times 10^{-3}$ m s^{-1}, an approximately westerly wind with the synoptic scale system vertical motion on the order of 10^{-3} m s^{-1}. The background radial velocity calculated using Eq. (1) was 6.83 m s^{-1}, and the innovation vector (the difference of observation and background) of the radial velocity was 10.17 m s^{-1}. Figure 2 presents the background wind field at the 7th level (∼4500 m): the single observation point and the radar site. Two parallel assimilation experiments were performed as follows: (1) Only radial velocity was used in experiment 1. (2) Both radial velocity and retrieved vertical ve-locity were used in experiment 2.

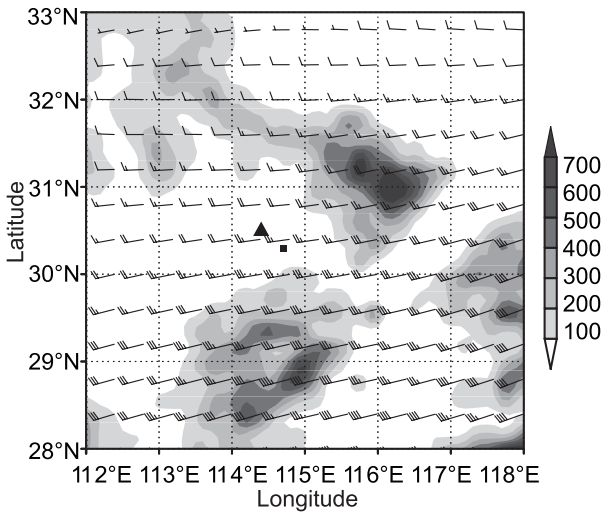

Fig. 2. Terrain (shaded, m) and background wind on the 7th level (Each long bar represents 4 m s^{-1}, ▲ represents radar site, ■ represents the observation point).

4.1 *Assimilating only radial velocity*

Figure 3 shows the 3DVAR analysis increment response to the single Doppler radial velocity observation of experiment 1. The horizontal wind increment at the 7th level (Fig. 3b) indicates that the very strong northwesterly wind was produced around the observation point, and that the maximum increment was >6 m s^{-1}. The influence scale was determined by the background error length scales: 80 km in this experiment groups. The increment decreased in value as the vertical distance away from the observation point increased, but there was no significant difference in flow pattern (Fig. 3a, the 4th level, ∼1500 m; Fig. 3c the 10th level, ∼8000 m). This means that the northwesterly wind information contained in the single Doppler radial velocity was ingested and propagated into the analysis variables. The corresponding vertical velocity increment response from the single radial velocity observation was very small, on the order of only centimeters per second (Fig. 3d), reflecting only the magnitude of synoptic scale systems. These results suggest that the contribution of radial velocity at low elevations to vertical velocity is tiny.

4.2 *Assimilating radial velocity and vertical velocity*

Figure 4 shows the 3DVAR analysis increments from experiment 2 that assimilates the Doppler radial velocity as well as the retrieved vertical velocity. The joint assimilation of the radial wind and retrieved

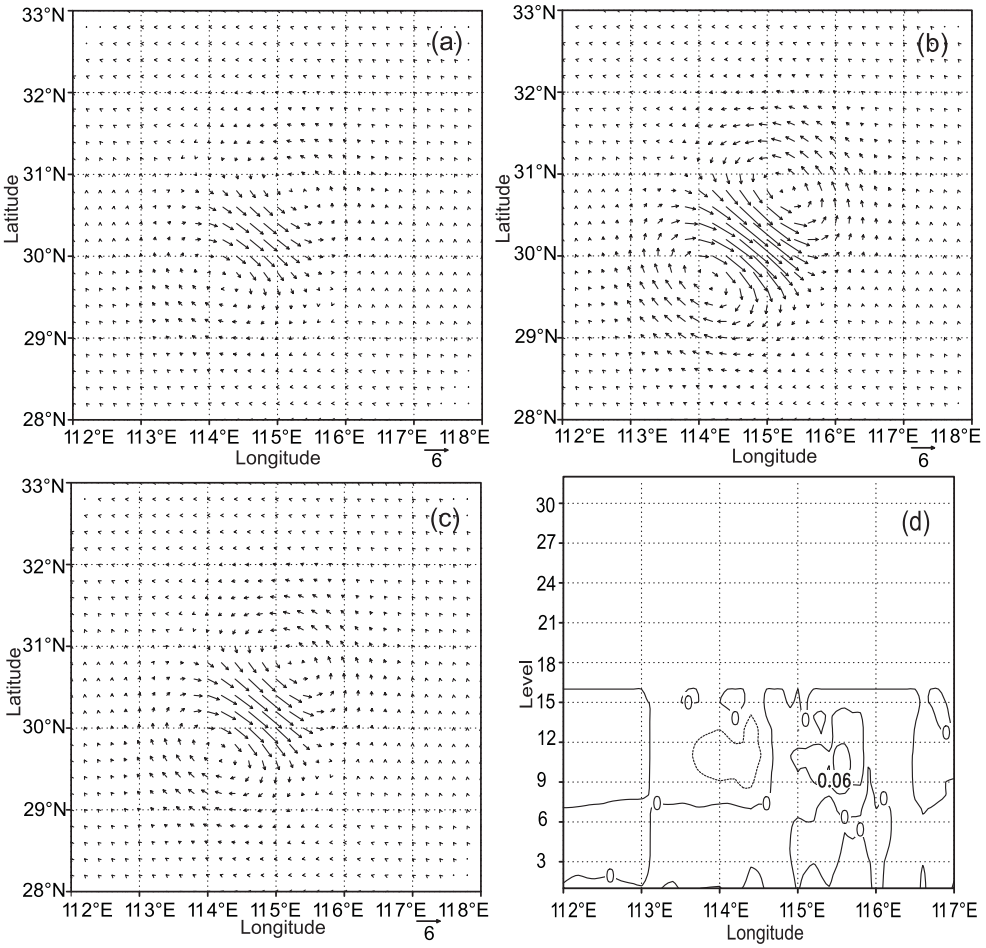

Fig. 3. Increments of experiment 1 (m s^{-1}), horizontal wind on (a) the 4th level, (b) 7th level, (c) 10th level, and (d) vertical section of vertical velocity along 30.5°N.

vertical velocity resulted in great changes in the flow patterns of the horizontal wind increments from low levels to high levels. Assimilation of retrieved vertical velocity, with the Richardson's equation as the observation operator, led to convergence on low levels and to divergence on high levels. Because the low levels were also affected by the terrain, the lower level wind increment presented a westerly flow (Fig. 4a). Because the middle level was the non-divergence layer, there was almost no change in the flow pattern on the middle level (Fig. 4b). By the divergence wind superposing the northwesterly wind, the high-level wind increment increased toward the southeast (Fig. 4c). The vertical velocity increment was very close to the observations, with the order of meters per second, reaching the magnitude of β-mesoscale weather systems (Fig. 4d). The results of this experiment indicate that assimilating retrieved vertical velocity could improve the analysis of β-mesoscale convective weather systems.

5. Typhoon case study

5.1 *Overview of Typhoon Sepat* (2007)

Typhoon Sepat (2007) landed on Chongwu (24.9°N, 118.9°E), Fujian province at 1800 UTC 18 August 2007, with the lowest pressure of 975 hPa and the maximum wind velocity of 33 m s^{-1} near the center (Fig. 5a). For the subsequent 12 h, accumulated rainfall at many stations in coastal areas exceeded 50 mm. Typhoon Sepat (2007) landed at mountainous areas where the altitudes range from 300 m to 1500 m, resulting in two rainfall centers at the windward slope due to an orographic effect. The maximum precipitation occurred at Zherong (27.24°N, 119.88°E) and Fuding (27.34°N, 120.20°E), with the values of 128 mm and 125 mm, respectively (Fig. 5b). The spiral cloud bands of the typhoon are obvious in the figure, with the width between 50 km and 100 km, in which several strong β-mesoscale convective structures are

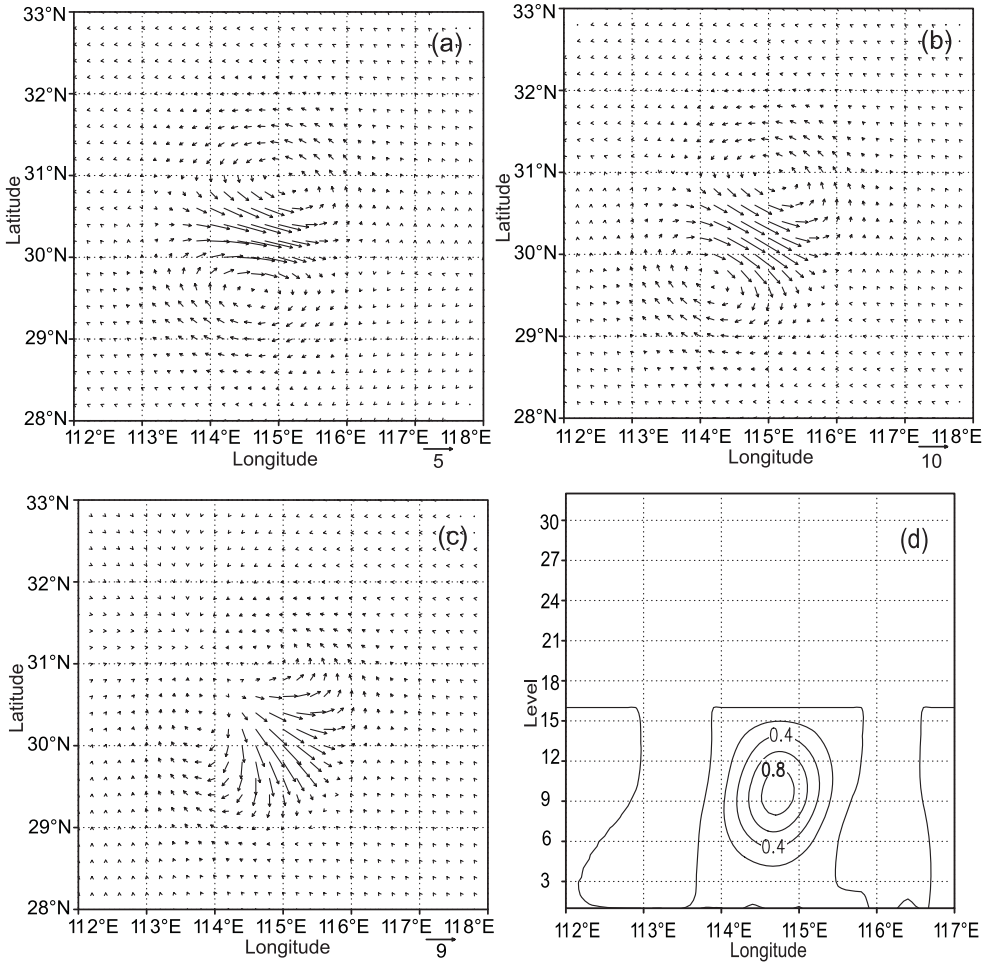

Fig. 4. Increments of experiment 2 (m s^{-1}), horizontal wind on (a) the 4th level, (b) 7th level, (c) 10th level, and (d) vertical section of vertical velocity along 30.5°N.

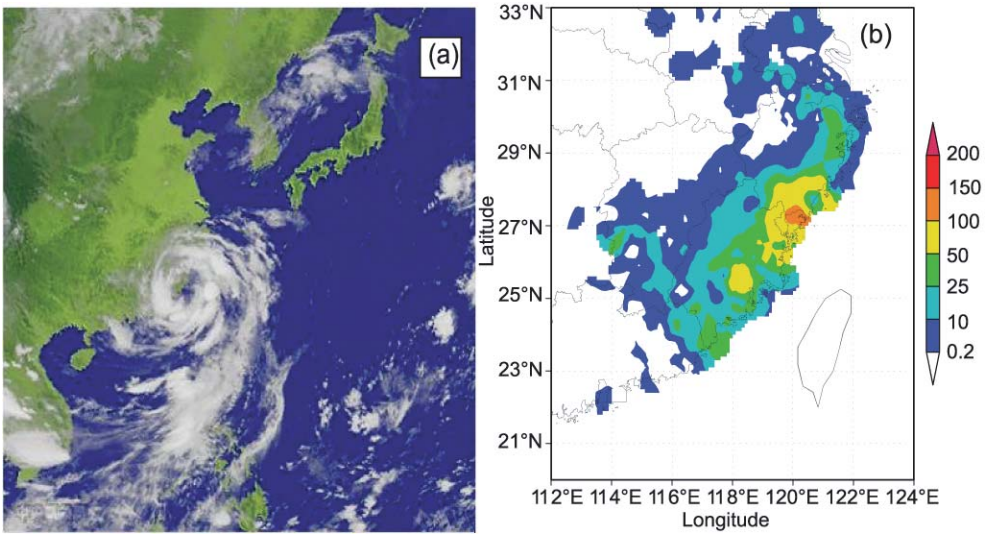

Fig. 5. Cloud image of Typhoon SEPAT (2007) (a) at 1800 UTC 18 August 2007 and (b) observed 12 h accumulated precipitation (mm) at 0600 UTC 19 August 2007.

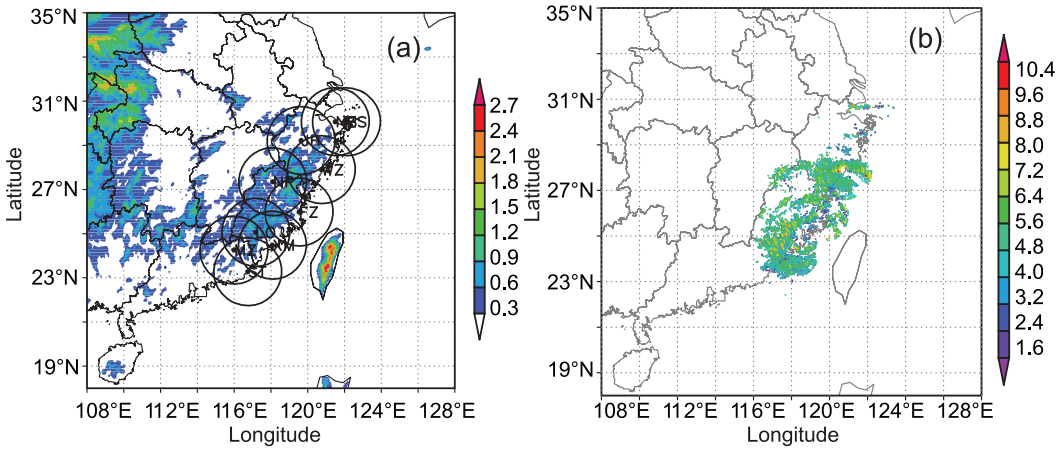

Fig. 6. (a) Terrain of model domain: • is radar site and ◯ is the maximum of unambiguous distance, and (b) radar observations after data thinning. (units: km)

embedded.

5.2 *Overview of the radar network*

The radar network consists of 10 S-band Doppler radars, Zhoushan (ZS), Ningbo (NB), Jinhua (JH) , Wenzhou (WZ), Nanping (NP), Fuzhou (FZ), Longyan (LO), Xiamen (XM), Meizhou (MZ) and Shantou (ST), which covered most of Typhoon Sepat (2007), except for the area far away from the coastline (Fig. 6a). Volumetric data from these radars were available every 6 minutes for nine elevation angles: 0.5°, 1.5°, 2.4°, 3.4°, 4.3°, 6.0°, 9.9°, 14.6°, 19.5°. Each elevation had ∼365 radials, while the resolutions of radar reflectivity and Doppler velocity on the radials were 1.0 km and 250 m, respectively. The unambiguous velocity range was ±26 m s^{-1}, and the unambiguous measurement range was 146 km. Data thinning and quality control were performed before the data assimilation. In this study, radar observations from 1 km to 10 km above the radar antenna and from 20 km away from radar site to the unambiguous measurement range were selected every 8 km along the radials. Furthermore, the selected point had to the two conditions that the absolute value of the radial velocity was >2 m s^{-1} (remove ground clutter and zero radial velocity line), and the radar reflectivity was >25 dBZ (remove clutter and stratus). As a result of these processes, a total of 8433 points were chosen, and the β-mesoscale convective systems were identified very clearly (Fig. 6b). The ambiguous velocities were de-aliased using a de-aliasing procedure according to the relationship between Nyquist velocity and radial velocity. Any ambiguous velocities that were left out by the procedure were eliminated by a further quality control step within the 3DVAR system. That is, the radial velocities with the absolute value of innovation (i.e., the difference of the model radial velocity and the observed radial velocity) >15 m s^{-1} were discarded.

5.3 *Modeling strategy*

Typhoon Sepat (2007) was simulated for 12 h after landing, from 1800 UTC 18 August to 1400 UTC 19 August 2007. All experiments were conducted over a grid mesh of 301×281 with grid spacing of 0.05°. The model top was 35 km with 32 vertical layers, and the time-step was 30 s. Physical schemes were as follows: NCEP-3 class scheme was used for explicit cloud; RRTM was used for long-wave radiation; the Dudhia scheme was used for shortwave radiation; MRF was used for the boundary scheme, and thermal diffusion was used for the land surface scheme. The background and lateral boundary came from the NMC forecast of T213.

5.4 *Sensitivity experiments*

A number of forecast experiments were conducted to examine the sensitivity of the forecast with respect to various changes of initial fields, which gained by

Table 1. Summary of experiments.

Experiment	Assimilated variables	Adjusting water vapor and cloud water of initial filed
CTRL	Control experiment, no radar data included	No
RV	Radial velocity data only	No
WR	Vertical velocity and rainwater mixing ratio	Yes
RVWR	Radial velocity, vertical velocity, and rainwater mixing ratio	Yes

different Doppler radar data assimilation strategies including radial velocity, or vertical velocity and rainwater mixing ratio, or both combined. The experiments are summarized in Table 1.

5.4.1 *Results of assimilating radar observations*

Using the 6-h forecast of T213 as the first guess, Fig. 7 shows the assimilating results of horizontal stream fields and divergence on 850 hPa and 500 hPa vertical velocity increment fields of experiments RV and RVWR. The horizontal flow is very smooth, with a clear typhoon vortex structure in the background field (Fig. 7a), but shows significant β-mesoscale convergence and divergence of horizontal wind near the center of the typhoon after assimilating radar data (Figs. 7b–d). The convergence and ascending areas corre-

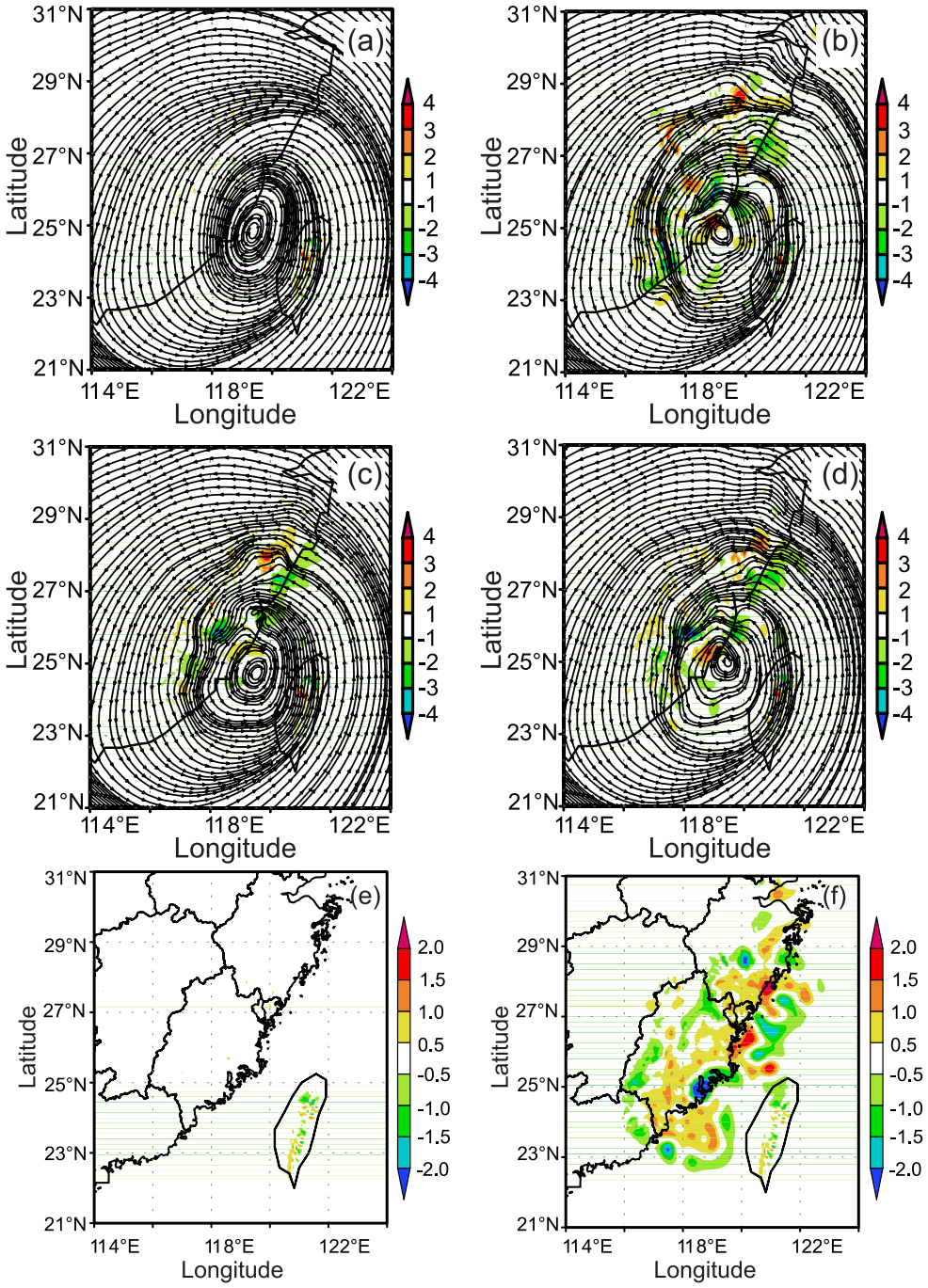

Fig. 7. Initial fields of the 850-hPa horizontal stream and divergence ($\times 10^{-4}$) for experiments (a) CTRL, (b) RV, (c) WR, (d) RVWR, and 500-hPa vertical velocity increment for (e) experiment RV and (f) experiment RVWR. (units: m s^{-1})

spond to the typhoon's spiral rain bands, while divergence and subsidence areas appear in the clear zone between the rain bands. These images indicate that the information of the β-mesoscale system of radar observations were rationally ingested into the analysis field. Despite the horizontal divergence of experiment RV, experiments WR and RVWR are on the same order of magnitude, but the vertical velocity increment of experiment RV is much smaller than that of experiments WR and RVWR (Figs. 7e and f). The result of experiment WR was similar to that of experiment RVWR (not shown); the maximum vertical velocity increment of experiment RVWR was >2.0 m s^{-1}. These results suggest that the assimilation of radial velocity can improve horizontal wind while assimilating retrieved vertical velocity mainly ameliorates the analysis of vertical movement in the initial fields.

5.4.2 12-h *typhoon track forecast*

Figure 8 presents the influence of radar data assimilation on the typhoon's path. Because the typhoon landed on mountainous areas with the altitudes rang ing from 300 m to 1500 m, the typhoon's center was located at the vortex center of 850 hPa. The track prediction of experiment CTRL was significantly different than the observations, especially in the early and later phrases. The errors seem small at the intermediate phrase, but that is because the typhoon's predicted speed was too fast. By only assimilating Doppler radar radial velocity, experiment RV greatly improved the typhoon track forecast, especially during the first several hours of the forecast. We believe the discrepancy during the later hours was, at least partly, caused by the uncertainty in determining the real position of the typhoon center, which is explained later in the paper. Assimilating vertical velocity and rainwater mixing ratio as well as adjusting water vapor and cloud water of the initial field, experiment WR had a little influence on the typhoon track forecast; the result looks similar to those of experiment CTRL to some extent. Jointly assimilating radial velocity, vertical velocity, rainwater and adjusting water vapor, and cloud water of the initial field, experiment RVWR improved the prediction of the typhoon track in the first several hours. This result is similar to that of experiment RV.

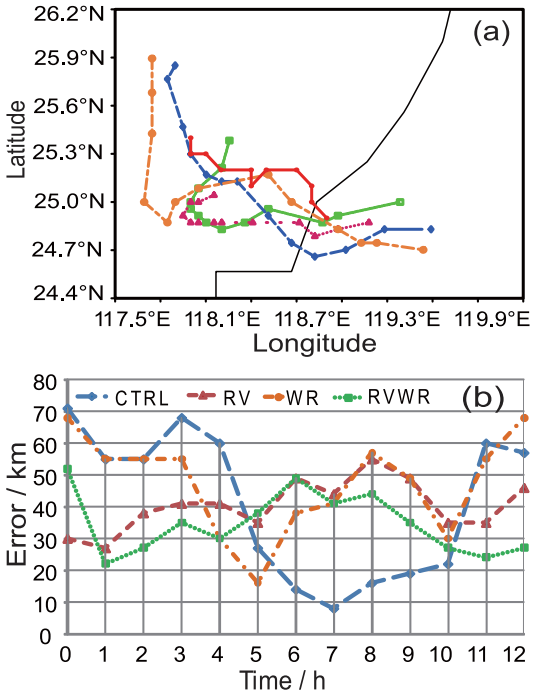

Fig. 8. Typhoon track forecast from 1800 UTC 18 Aug to 0600 UTC 19 Aug 2007 (a) •: OBS; ◇: CTRL; △ RV; ◯: WR; □ RVWR) and (b) track error of 12 h.

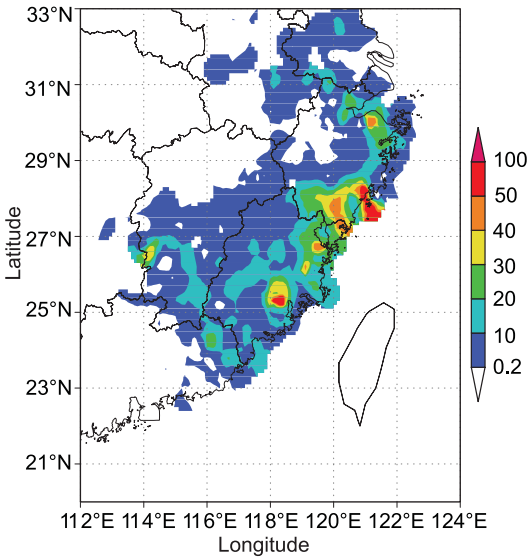

Fig. 9. Observed 6-h accumulated precipitation at 0600 UTC 19 August 2007. (units: mm)

In the latter 6 h, the typhoon's eye was not well identifiable due to ground friction, thus it was difficult to accurately determine the center of the typhoon. On the other hand, the observed best track was based on large-scale analysis without the consideration of radar observations, which may not have accurately represented the real typhoon center. With destruction of the typhoon eye, the radar reflectivity images revealed that a strong reflectivity center remains around the point (25°N, 118°E), which is shown by the 6-h accumulated precipitation at 0600 UTC 19 August 2007 in Fig. 9. Possibly, the vortex center in the simulations corresponds to this precipitation system, which caused the backward curving of the vortex centers of experi-

ments RV and RVWR, as shown in Fig. 8a.

5.4.3 12-h *accumulated precipitation forecast*

Figure 10 depicts a comparison of accumulated precipitation within the first 12 h of the four assimilation and forecast experiments. Taking the 6-h forecast of T213 as the initial field, the 12-h accumulated precipitation forecast of experiment CTRL is acceptable (Fig. 10a). To some extent, this can be attributed to the good humidity conditions (RH >80% in initial field) and the lifting effect of the terrain.

By only assimilating Doppler radar radial velocity, the forecast result of the accumulated precipitation of experiment RV (Fig. 10b) is similar to the result of experiment CTRL. Therefore, although the assimilation of radial wind can improve the β-mesoscale analysis of horizontal wind, temperature and pressure in the initial field and enhance convergence and divergence, without the support from condensation and its associated updraft, the mesoscale dynamic information is difficult to maintain in a dry background.

Assimilating vertical velocity and rainwater mixing ratio, both derived from the radar reflectivity factor, and adjusting vapor and cloud water of initial field, ex experiment WR yielded a forecast that was closer to observations than experiment CTRL in terms of 12-h accumulated precipitation, especially with regard to the distribution of the torrential precipitation (Fig. 10c). This is due to the condensation of saturated water vapor in the initial field. With the rising motion, the condensation released latent heat and heats the atmosphere. Through the buoyancy effect, the mesoscale convective structure was established, maintained, and developed quickly. In addition, the hydrometeors in the initial field also made a certain contribution to the precipitation.

Experiment RVWR assimilated radial velocity, vertical velocity and rainwater together, provides the best

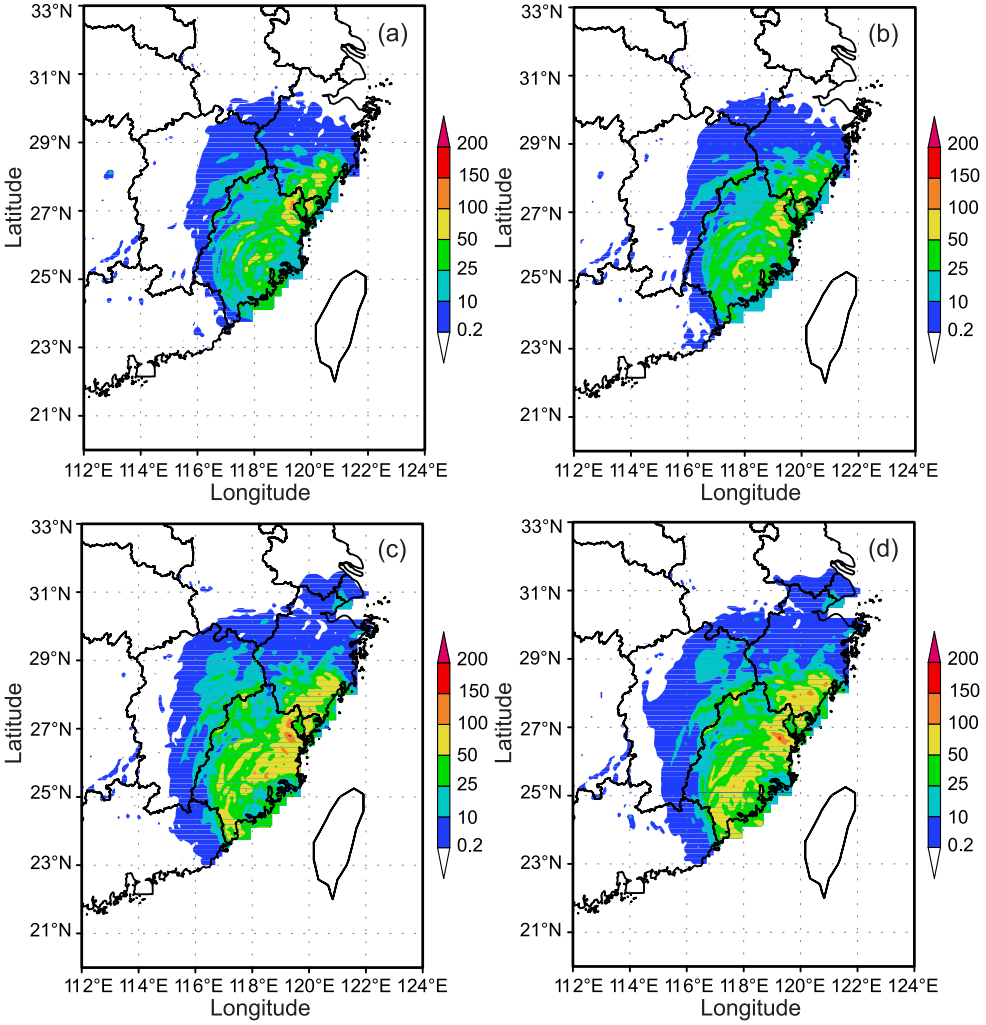

Fig. 10. Twelve-hour accumulated precipitation forecast at 0600 UTC 19 August 2007 of experiments (a) CTRL, (b) RV, (c) WR, and (d) RVWR. (units: mm)

forecast of 12-h accumulated precipitation (Fig. 10d), but the precipitation intensity only increased slightly, and precipitation distribution was a little different compared with experiment WR.

This analysis shows that assimilating only the radial wind improves mainly the horizontal wind in the initial field but has little effect on the 12-h accumulated precipitation. When the derived vertical velocity and rainwater were assimilated along with the adjustment of vapor and cloud water in the initial field, the mesoscale convective system structure improved, resulting in large impact on the 12-h accumulated precipitation.

5.4.4 1-h *accumulated precipitation forecast and quantitative precipitation verification*

Figure 11 shows the effect of radar data assimilation to reduce the spin-up problem of precipitation forecast.

Doppler radar radial wind data assimilation can increase the mesoscale information in initial fields and can trigger mesoscale precipitation to some extent, the accumulative rainfall within 1 h (Fig. 11b) was stronger than the control run (Fig. 11a). This lasted ∼3 h. However, because of the lack of the support of continued thermodynamic effect, there was no precipitation in some mesoscale convergence zones. Assimilating vertical velocity and rainwater mixing ratio as well as adjusting vapor and cloud water initialized the model with strong precipitation, and the precipitation system was developed and maintained (Fig. 11c). At the 3rd forecast hour, the precipitation was still stronger than in experiment CTRL obviously, and this advantage disappeared largely at the 6th hour. The precipitation forecast was very close to the observations (Fig. 11e), and the spin-up phenomenon was eliminated to a large extent. Experiment RVWR was similar to experiment WR with a slightly stronger 1-h accumulated precipitation forecast (Fig. 11d).

CSI and bias scores of forecasts in the first 6-h are presented in Fig. 12, because after the 6th hour, the differences among the experiments were small. The observed precipitation was interpolated to forecast grid points, and precipitation in the sea was blocked out. The accumulation of precipitation was greater than or equal to the prescribed cutoff values of 0.1 mm, 5 mm (for the 1-h and 3-h forecasts, respectively), 10 mm (for the 6-h forecasts), 15 mm (for the 3-h forecasts), 25 mm (for the 6-h forecasts).

The CSI scores in these figures indicate that the 1-h accumulated precipitation forecast skills from experiment WR and experiment RVWR were generally better than those of experiment CTRL in the first 2 h, for both thresholds of <5 mm h^{-1} and >5 mm h^{-1}, and that experiment RV was better than experiment CTRL in the forecast of precipitation >5 mm h^{-1} until the 6th hour. The 3-h accumulated precipitation forecast skill of experiments RV, WR, and RVWR were better than those of experiment CTRL at all thresholds. The 6-h accumulated precipitation forecast skill of experiments RV, WR, and RVWR were better than those of experiment CTRL at the thresholds <10 mm h^{-1} and >25 mm h^{-1}, but they were worse at the threshold <25 mm h^{-1}.

The ideal bias is exactly "1" across all categories. The 1-h accumulated precipitation bias scores of experiments RV, WR, and RVWR were generally better than those of experiment CTRL in the full forecast periods at the <5 mm h^{-1} threshold, except the 6th hour. At >5 mm h^{-1}, experiments WR and RVWR were better than experiment CTRL, but with a significantly false prediction ratio, and this trend was worse at the 4th hour. In the 3-h and 6-h accumulated precipitation forecasts, the bias scores improved almost at all thresholds, but with a obviously false prediction ratio at small amount precipitation, also.

This analysis shows that, although the assimilation of radial wind makes little improvement to precipitation, it can greatly improve the forecast of typhoon track. Therefore, assimilating radial velocity, vertical velocity, and rainwater together, simultaneously adjusting vapor and cloud water of the initial field, would advance the forecasts of both precipitation and typhoon track.

6. Conclusions

This study investigated the Doppler radar data 3DVAR assimilation technique of GRAPES model and the results of single-point experiments and sensitivity experiments on a real typhoon case. The main conclusions are summarized as follows:

(1) Doppler radar radial wind assimilation mainly improves the horizontal wind over the background field, which consequently improves the mass field by geostrophic relations, but has little effect on vertical motion. The magnitude of the analyzed vertical velocity is at the order of centimeters per second, reflecting the vertical motion of the synoptic-scale weather system.

(2) Using the Richardson's equation as the observation operator to assimilate the vertical velocity (retrieved from radar reflectivity factor) improves the analysis of the three-dimensional dynamic field, resulting in strong vertical motion of the β-mesoscale weather system. However, the impact of the vertical velocity assimilation on horizontal wind and mass field is relatively small, probably because the balances

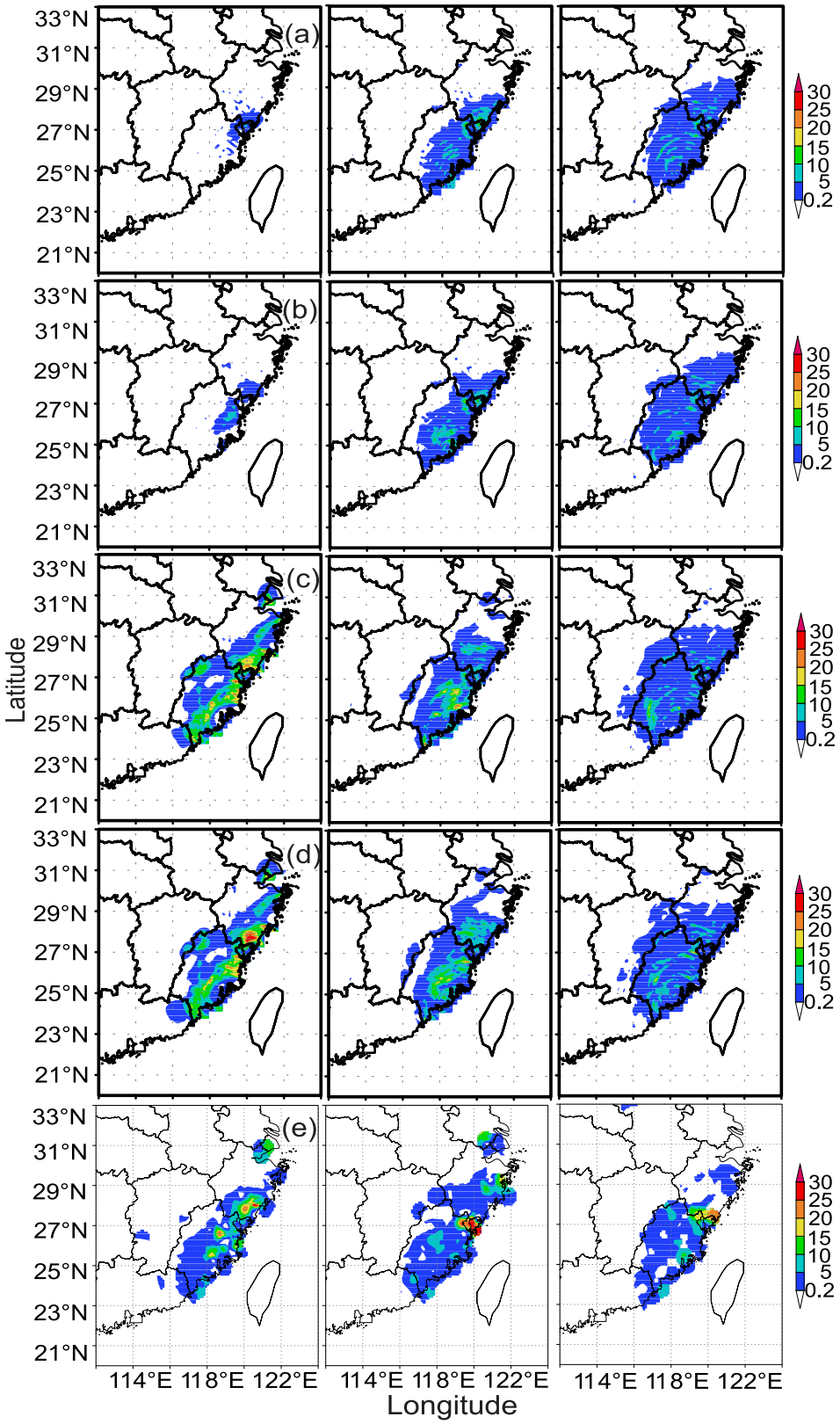

Fig. 11. One-hour accumulated precipitation in the 1st hour (left), 3rd hour (middle), and 6th hour (right) of experiments (a) CTRL, (b) RV, (c) WR, (d) RVWR, and (e) observations. (units: mm)

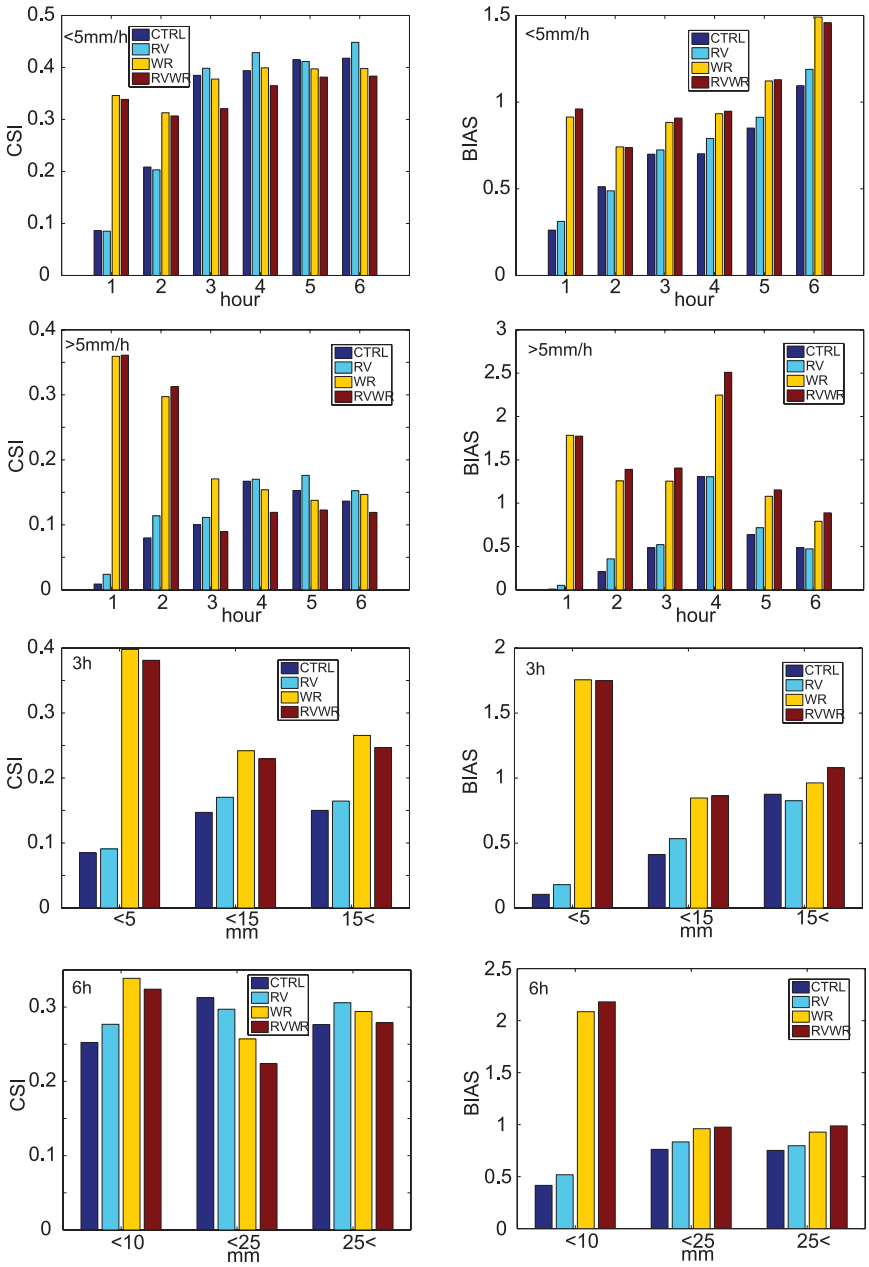

Fig. 12. CSI and bias scores of 1-h, 3-h, and 6-h accumulated precipitation for experiments CTRL, RV, WR, and RVWR.

used in the 3DVAR system are not suitable for the β-mesoscale weather system.

(3) The typhoon experiments indicate that assimilating Doppler radial velocity greatly improves the forecast of typhoon track and improves trigger β-mesoscale precipitation to some extent. Assimilating vertical velocity and rainwater mixing ratio, simultaneously adjusting vapor and cloud water of initial field, significantly improves the forecast of typhoon precipitation and removes the spin-up phenomenon, but it has little effect on typhoon track forecasting.

Joint assimilation of Doppler radial velocity, vertical velocity, and rainwater mixing ratio, and simultaneously adjusting vapor and cloud water of initial field, improves both precipitation and typhoon track forecasts.

(4) The incomplete coverage of the typhoon system by the radar observations affect the simulation results to some extent.

This study mainly aimed to investigate a β-

mesoscale convective weather system. As such, the parameters in the vertical velocity retrieval technique were set for such systems. Taking into account the varied scales of weather systems and the representation of observation data, different statistical calculations should be performed for different weather systems. Moreover, how to set the ratios of rotation and convergence and the parameters of geostrophic and non-geostrophic horizontal wind require further in-depth study.

(5) Different scales of weather systems generally use different modes, or different mode settings, presently. The technique developed in this study is designed mainly for the summer β-mesoscale convective weather systems; such weather systems have similar characteristics. For severe convective weather systems with γ-mesoscale, the model resolution, the parameters in Eq. (2), and even the length scaling from background error need to be adjusted. If it is applied to large-scale stratiform rain in winter, Eq. (2) must be reconstructed.

Acknowledgements. This research was supported by the National Key Scientific and Technological Project (Grant No. 2006BAC02B00), and National Natural Science Foundation of China (Grant No. 40518001). Special thanks are given to Dr. Jenny Sun from NCAR for valuable comments and careful revision to the paper.

REFERENCES

Biggerstaff, M. I., and R. A. Houze, Jr., 1991: Kinematic and precipitation structure of the 10–11 June 1985 squall line. *Mon. Wea. Rev.*, **119**, 3034–3065.

Browning, K A., 1989: The mesoscale data base and its use in mesoscale forecasting. *Quart. J. Roy. Meteor. Soc.*, **115**, 717–762.

Byrom, M., and I. Roulstone, 2002: Calculating vertical motion using Richardson's equation. ECMWF/GEWEX Workshop on Humidity Analysis, UK, European Centre for Medium Range Weather Forecasts, 49–57.

Caya, A., J. Sun, and C. Snyder, 2005: A comparison between the 4D-Var and the ensemble Kalman filter techniques for radar data assimilation. *Mon. Wea. Rev.*, **133**, 3081–3094.

Chen, D., and Coauthors, 2008: New generation of multiscale NWP system (GRAPES): General scientific design. *Chinese Science Bulletin*, **53**, 3433–3445.

Gu, J., Y. H. Kuo, D. M. Barker, J. Xue, and X. Ma, 2005: Assimilation and simulation of Typhoon Rusa (2002) using the WRF system. *Adv. Atmos. Sci.*, **22**, 415–427.

Guo, Y. R., Y. H. Kuo, J. Dudhia, D. Parsons, and C. Rocken, 2000: Four-dimensional variational data assimilation of heterogeneous mesoscale observations for a strong convective case. *Mon. Wea. Rev.*, **128**, 619–643.

Haase, G., S. Crewell, C. Simmer, and W. Wergen, 2000: Assimilation of radar data in mesoscale models: Physical initialization and latent heat nudging. *Physics and Chemistry of Earth* (B), **25**, 1237–1242.

Hoke, J. E., and R. A. Anthes, 1976: The initialization of numerical models by a dynamic relaxation technique. *Mon. Wea. Rev.*, **104**, 1551–1556.

Kishore Kumar, K., A. R. Jain, and D. Narayana Rao, 2005: VHF/UHF radar observations of tropical mesoscale convective systems over southern India. *Ann. Geophys.*, **23**, 1673–1683.

Koizumi, K., Y. Ishikawa, and T. Tsuyuki, 2005: Assimilation of precipitation data to the JMA mesoscale model with a four-dimensional variational method and its impact on precipitation forecasts. *SOLA*, **1**, 45–48.

Lee, J. H., H. H. Lee, Y. H. Choi, H. W. Kim, and D. K. Lee, 2010: Radar data assimilation for the simulation of mesoscale convective systems. *Adv. Atmos. Sci.*, **27**, 1025–1042. doi: 10.1007/s00376-010-9162-8.

Liu, H., H. Xu, J. Xue, Z. Hu, and T. Shen, 2008a: Radar reflectivity factor applied to initialize cloud-resolving mesoscale model. Part I: Retrieval microphysics elements and vertical velocity. *Acta Meteorologica Sinica*, **22**, 162–172.

Liu, H., H. Xu, J. Xue, Z. Hu, and T. Shen, 2008b: Radar reflectivity factor applied to initialize cloud-resolving mesoscale model. Part Ⅱ: Numerical simulation experiments. *Acta Meteorologica Sinica*, **22**, 173–186.

Marecal, V., and J. F. Mahfouf, 2003: Experiments on 4D-Var assimilation of rainfall data using an incremental formulation. *Quart. J. Roy. Meteor. Soc.*, **129**, 3137–3160.

Mcginley, J. A., and J. R. Smart, 2001: On providing a cloud-balanced initial condition for diabatic initialization. Preprints, *14th Conf. on Numerical Weather Prediction*, Fort Lauderdale, FL, Amer. Meteor. Soc., 40–44.

Milan, M., F. Ament, V. Venema, and C. Simmer, 2005: Physical initialization to incorporate radar precipitation data into a numerical weather prediction model (Local Model). *32nd Conference on Radar Meteorology/11th Conference on Mesoscale Processes*, Albuquerque, NM, AMS, JP1 J.15, 1–5.

Richardson, L. F., 1922: *Weather Prediction by Numerical Process*. 1st ed., Cambridge University Press, 236pp.

Snyder, C., and F. Zhang, 2003: Assimilation of simulated Doppler radar observations with an ensemble Kalman filter. *Mon. Wea. Rev.*, **131**, 1663–1677.

Sun, J., 2005a: Initialization and numerical forecasting of a supercell storm observed during STEPS. *Mon. Wea. Rev.*, **133**, 793–164.

Sun, J., 2005b: Convective-scale assimilation of radar data: Progress and challenges. *Quart. J. Roy. Meteor. Soc.*, **131**, 3439–3463.

Sun, J., and N. A. Crook, 1997: Dynamical and micro-

physical retrieval from Doppler radar observations using a cloud model and its adjoint. Part I: Model development and simulated data experiments. *J. Atmos. Sci.*, **54**, 1642–1661.

Sun, J., and N. A. Crook, 1998: Dynamical and microphysical retrieval from Doppler radar observations using a cloud model and its adjoint. Part Ⅱ: Retrieval experiments of an observed Florida convective storm. *J. Atmos. Sci.*, **55**, 835–852.

Wan, Q., J. Xue, and S. Zhuang, 2006: Study on the variational assimilation technique for the retrieval of wind fields from Doppler radar data. *Acta Meteorologica Sinica*, **10**, 1–19.

Wang, X., M. K. Yau, B. Nagarajan, and L. Fillion, 2010: The impact of assimilating radar-estimated rain rates on simulation of precipitation in the 17–18 July 1996 Chicago Floods. *Adv. Atmos. Sci.*, **27**, 195–210, doi: 10.1007/s00376-009-8212-6.

Xiao, Q., Y. H. Kuo, J. Sun, W. C. Lee, E. Lim, Y. R. Guo, and D. M. Barker, 2005: Assimilation of Doppler radar observations with a regional 3DVAR system: Impact of Doppler velocities on forecasts of a heavy rainfall case. *J. Appl. Meteor.*, **44**, 768–788.

Xiao, Q., Y. H. Kuo, J. Sun, W. C. Lee, D. M. Barker, and E. Lim, 2007: An approach of radar reflectivity data assimilation and its assessment with the inland QPF of Typhoon Rusa (2002) at landfall. *J. Appl. Meteor. Climatol.*, **46**, 14–22.

Xu, X., L. Liu, and G. Zheng, 2005: Dynamical and microphysical retrieval from simulated Doppler radar observations using the 4DVAR assimilation technique. *Acta Meteorologica Sinica*, **19**, 160–173.

Xue, J., S. Zhuang, G. Zhu, H. Zhang, Z. Liu, Y. Liu, and Z. Zhuang, 2008: Scientific design and preliminary results of three-dimensional variational data assimilation system of GRAPES. *Chinese Science Bulletin*, **53**, 3446–3457.

Yang, Y., C. Qiu, J. Gong, and J. Huang, 2009: The WRF 3DVar system combined with physical initialization for assimilation of Doppler radar data. *Acta Meteorologica Sinica*, **23**, 129–139.

Yuter, S. E., and R. A. Houze, Jr., 1995: Three-dimensional kinematic and microphysical evolution of Florida cumulonimbus. Part II: Frequency distribution of vertical velocity, reflectivity, and differential reflectivity. *Mon. Wea. Rev.*, **123**, 1941–1963.

Yuter, S. E., and R. A. Houze, Jr., 2003: Microphysical modes of precipitation growth determined by S-band vertically pointing radar in orographic precipitation during MAP. *Quart. J. Roy. Meteor. Soc.*, special MAP issue, **129**, 455–476.

Zhang, F., C. Snyder, and J. Sun, 2004: Impacts of initial estimate and observations on convective-scale data assimilations. *Mon. Wea. Rev.*, **132**, 1238–1253.

Zupanski, M., D. Zupanski, D. F. Parrish, E. Rogers, and G. DiMego, 2002: Four-dimensional variational data assimilation for the blizzard of 2000. *Mon. Wea. Rev.*, **130**, 1967–1988.